Original Research Article: full paper

(2022), «EUREKA: Physics and Engineering»
Number 5

STUDY OF INTERFERENCE FIT BETWEEN STEEL AND BRASS PARTS

Nguyen Huu Loc✉
Department of Machine Design[1,2]
nhloc@hcmut.edu.vn

Lam Vi Phong
Department of Machine Design[1,2]

[1]*Ho Chi Minh City University of Technology (HCMUT)*
268 Ly Thuong Kiet str., District 10, Ho Chi Minh City, Vietnam, 700000

[2]*Vietnam National University Ho Chi Minh City*
Linh Trung Ward, Thu Duc City, Ho Chi Minh City, Vietnam, 700000

✉**Corresponding author**

Abstract

Interference fits are generally used in mechanical systems because they have low-cost production and their assembly parts are much smaller than other mechanical joints. Also, their geometric shapes and material properties allow technicians to actively determine how strong the fits are. In this study, let's present research on interference fits between steel and brass assembly parts. The experimental processes were accomplished with five pairs of specimens to evaluate the behaviours of surface asperities under a high loading condition. Specifically, the specimen pair includes a C45 steel shaft and a C2680 brass hub, which have different surface roughness values (*Ra*). Let's apply high-precision methods in measuring all dimensional parameters and employed axial load tests for distinctively inspecting the steel-brass interference fit performance. In every experiment, the measured responses are:

1) the surface roughness values (*Ra*) before and after loading cycles;

2) the axial load (F_a);

3) the relative displacement value or the real-time interface length in loading stages (l).

The aim of this study is to propose a new relative interference value specifically between steel and brass assembly parts, which can help determine the interference loss value more accurately. It was concluded that with the relative interference of 2.25 ‰ the load capability of steel-brass interference fits is extended. Besides, let's narrow down the predictive loss coefficient (a) for steel-brass interference assemblies ranging from 1.1 to 2.1, which varies from widely used standards considering $a = 3$. This result helps minimize inaccuracies in interference fit designs, calculations, and work capabilities.

Keywords: interference fit, relative interference, interference fit loss coefficient, steel, brass, surface roughness, load capability.

DOI: 10.21303/2461-4262.2022.002524

1. Introduction

Most investigations on interference fits engage in studying theoretical problems to resolve practical load strength limitations. Besides, many researchers have developed empirical approaches whose results help to find sufficient geometric parameters that expectedly fulfill any engineering requirements. Therefore, we may need to discover more technological solutions to enhance the reliability of interference fits.

The basis of interference fits [1] is based on theories of materials elasticity, especially Lame's equations for thick-wall cylinders. They are also the groundwork of current interference fit calculation guidelines and standards, such as DIN 7190-1 [2] or ISO 286-1 [3] equivalently.

The interface pressure directly symbolizes the interference fit strength, but it is not easy, even unattainable, to precisely evaluate this value. Thus, researchers present indirect procedures that reflect this aspect as holding force or holding torque, or sometimes, a combination of both. A new accurate way to predict the interference fit strength was proposed by considering the influence of non-contact regions, which are hard to be evaluated with standard calculating methods [4]. Another study has drawn some ground-breaking conclusions related to the fatigue of interference fit under varieties of torque loading cycles [5].

As mentioned above, practical research problems play a vital role in this distinct scientific field. Generally, the studies revolve around the factors affecting the interference fit load capability, such as the coefficient of friction [6–8], contact surface condition [9, 10], geometrical figures [11–13], coupling materials properties, loading condition [14], working environment, and assembly procedure.

Genuinely, studies of interference fit comprehend an abundance of technological subjects, from theoretical topics to practical problems. However, most of them center on the typical case of steel-steel assemblies. So, there are more or less research gaps in couplings between steel and nonferrous alloy parts or mutually amongst nonferrous alloy parts.

This paper distinctively highlights the study of interference fit between steel and brass assembly parts. Commonly, this material pair has applications in: worm gear construction – mounting worm wheel body and worm wheel rim, sliding bearing construction – bearing bush and machine body. In this case, the employment of interference fit optimizes the size of assembly parts, consequently lowering the manufacturing costs compared to traditional connections.

As previously said, regularly, researchers indirectly observe the interference fit load-bearing capability by measuring the actual holding force or holding torque value. This calculation was discussed in numerous studies, in which they equally considered the fit load-bearing strength as the interface static friction limit [15].

Expressly, there is the following formula:

$$F_{\max} = 2\pi \cdot r_f \cdot l \cdot p_f \cdot \mu, \tag{1}$$

where $F_{\max}$ is the interference fit maximum load-bearing strength, r_f is the nominal interface radius, l is the actual length of the contact area between coupled parts, p_f is the interface pressure, and μ is the coefficient of friction referring to the mating materials and other crucial factors, especially for steel-brass connection, μ ranges from 0.17 to 0.25 as various contact forms [2, 3].

Furthermore, investigators occasionally represent $F_{\max}$ as a composition of the interface axial and circumferential force, respectively expressed as F_a and F_c [15]:

$$F_{\max} = \sqrt{F_a^2 + F_c^2}. \tag{2}$$

In some loading cases, let's observe axial and circumferential (as torsion T) influences separately. In other words, the interference fit is only affected by a single load component, thereby, $F_{\max} = F_a$ or contrary $F_{\max} = F_c = T/r_f$.

From (1), (2), let's achieve a correlation between interface pressure and loading components, considering a particular surface point:

$$p_f = \frac{\sqrt{F_a^2 + F_c^2}}{2\pi \cdot r_f \cdot l \cdot \mu}. \tag{3}$$

Additionally, from the basis of thick-walled cylinders [1] to the revisions of several researchers [15], it is possible to easily point out the relation between the contact surface pressure and the interference fit characteristic parameters, shown as the following formula:

$$p_f = \frac{\delta}{2r_f \left[\frac{r_f^2 + r_i^2}{E_s \cdot \left(r_f^2 - r_i^2\right)} - \frac{\nu_s}{E_s} + \frac{r_o^2 + r_f^2}{E_h \cdot \left(r_o^2 - r_f^2\right)} + \frac{\nu_h}{E_h} \right]}, \tag{4}$$

where δ is the fit interference value, r_i is the shaft inner radius, r_o is the hub outer radius, E_s, ν_s are respectively Young's modulus and Poisson's ratio of the shaft material, E_h, ν_h are respectively Young's modulus and Poisson's ratio of the hub material.

With (3), (4), let's acquire a connection between the affecting loads and the interference fit representative elements:

$$\sqrt{F_a^2 + F_c^2} = \frac{\delta \cdot \pi \cdot l \cdot \mu}{\frac{1}{E_s} \cdot \left(\frac{r_f^2 + r_i^2}{r_f^2 - r_i^2} - \nu_s \right) + \frac{1}{E_h} \cdot \left(\frac{r_o^2 + r_f^2}{r_o^2 - r_f^2} + \nu_h \right)}, \quad (5)$$

in this case of applying the axial load testing method, $F_c = 0$:

$$F_a = \frac{\delta \cdot \pi \cdot l \cdot \mu}{\frac{1}{E_s} \cdot \left(\frac{r_f^2 + r_i^2}{r_f^2 - r_i^2} - \nu_s \right) + \frac{1}{E_h} \cdot \left(\frac{r_o^2 + r_f^2}{r_o^2 - r_f^2} + \nu_h \right)}. \quad (6)$$

Besides, most interference fit calculation principles assume the actual interference losses are critical [2, 3], which can help predict the load-bearing strength precisely and select the most proper fit regarding technological requirements. In short, it is possible to describe the practical interference value under the following formula:

$$\delta = \delta_m - L_\delta = \delta_m - \left(L_r + L_p \right), \quad (7)$$

where δ_m is the actual mean interference value, L_r is the interference loss depending on the surface roughness, and L_p is the interference loss caused by the plastic deformation of mating parts.

Primarily, L_r exists in every interference fit situation, which is the effect of the reaction between assembly surfaces under high contact pressure. In other words, the flattening of surface asperities happens and influences the surface roughness value of assembly parts, the coupling coefficient of friction, and the fit load-bearing capability [2, 3]. It is possible to define L_r as:

$$L_r = a \cdot \left(Ra_s + Ra_h \right), \quad (8)$$

where a is the loss factor, which varies among different interference fits, and researchers commonly choose this value to be 3 if there are no specified preconditions [2, 3], Ra_s is the shaft assembly surface roughness value, and Ra_h is the hub assembly surface roughness value.

Next, it is necessary to consider the L_p value due to the plastic deformation of assembly parts, the primary cause which comes from the hardening of surface asperities. More specifically, when the joint surfaces interact with each other, the first deformation will be the surface asperities; but when the deformation reaches a certain value, the asperities will not be able to deform further [16]. At this time, if the interface pressure is large enough, bulk deformation of the joint elements will happen. In practice, researchers use a coefficient to predict the appearance of L_p, which is a ratio of the actual mean interference value δ_m to the nominal diameter of the fit d, also known as the relative interference δ_m/d. Regarding some relevant studies, L_p will possibly become noticeable when the relative interference gets to the rate of 1.6 ‰ [17].

Finally, it is possible to thoroughly investigate the relationship between the axial load and the joint distinctive factors under the formula below:

$$F_a = \frac{\left[\delta_m - a \cdot \left(Ra_s + Ra_h \right) - L_p \right] \cdot \pi \cdot l \cdot \mu}{\frac{1}{E_s} \cdot \left(\frac{r_f^2 + r_i^2}{r_f^2 - r_i^2} - \nu_s \right) + \frac{1}{E_h} \cdot \left(\frac{r_o^2 + r_f^2}{r_o^2 - r_f^2} + \nu_h \right)}. \quad (9)$$

As it is possible to see, the loss factor a and the interference loss caused by plastic deformation L_p are crucial. In some situations, it is necessary to evaluate these values carefully to reduce inaccuracies in designing interference fit. Let's assume that, for the steel-brass joint, the relative interference value δ_m/d is different from the case of the steel-duralumin joint in [17], which brings different values of the loss factor a and the interference losses L_r, L_p. Here, the real problem is that we could not use the general calculation standards for specific important cases of assemblies between steel and other metallic alloys. So this study aims to identify these specific values by analyzing the experimental results of the interference fit axial load test.

2. Materials and methods

2. 1. Material pair

As previously said, the empirical objective of this study is to identify the relative interference value δ_m/d of the steel-brass interference fit, then calculate the interference losses L_r and L_p. Besides, there are also conclusions about the behaviors of surface asperities for this particular coupling material pair.

This paper investigates the case of cylindrical interference fit between a C45 steel shaft and a C2680 brass hub. The nominal diameter of the mating parts d is 20 mm, and their geometrical tolerances for the inner and outer parts are shown in **Fig. 1** in detail with other parameters. Additionally, the standard surface roughness values are Ra 2.5 for the shaft and Ra 0.63 for the hub.

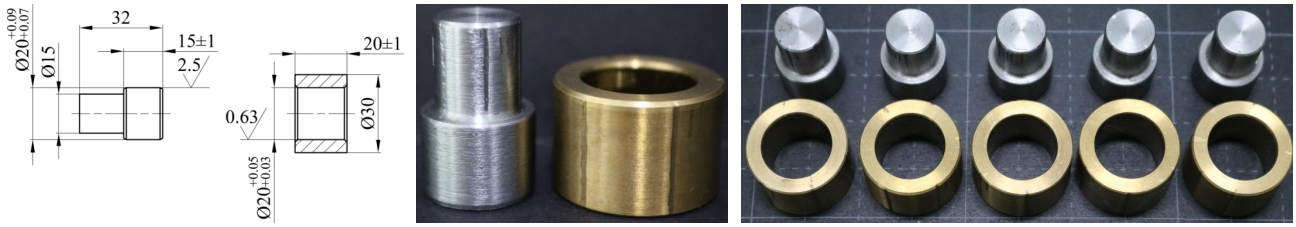

a *b* *c*

Fig. 1. Experimental specimens: *a* – dimensional parameters; *b*, *c* – actual pairs of specimens

In the machining process of experimental specimens, we ensured their theoretically determined mechanical properties by strictly examining the raw workpieces. The inspection results of the input materials all met the guidelines of DIN EN 10277 [18] and DIN EN 12163 [19] for shaft and hub specimens, respectively. **Table 1** shows the standard mechanical properties of shaft and hub specimens.

Table 1

Mechanical properties of shaft and hub specimens

Specimen	Density	Poisson's ratio	Young's modulus	Material yield strength
	ρ	ν	*E*	σ_y
	(kg/m^3)	–	(GPa)	(MPa)
Shaft (C45 steel)	7850	0.3	210	360
Hub (C2680 brass)	8500	0.34	112	240

After machining, let's carefully inspect the samples, selected five pairs of the most suitable parts, then assembled them using a universal testing machine (UTM).

2. 2. Measuring of geometrical parameters

In this article, let's consider the actual interference value as the difference between the outer diameter of the shaft and the inner diameter of the hub. Since the interference value directly affects the characteristics and load capability of the fit, it is necessary to evaluate the real diameter value of joint elements with high accuracy methods.

Here, the mounting diameter of the hub was measured using the Mitutoyo Beyond Apex 504 coordinate-measuring machine at two different cross-sectional positions perpendicular to the part length H, at $H = 10$ mm and $H = 15$ mm. Moreover, let's investigate the contact surface of the experimental specimens at multiple positions by employing the Mitutoyo SJ-301 surface profiler. The obtained values were mainly in the range of $0.5 \leq Ra \leq 0.85$ μm. **Fig. 2** presents the equipment used in this experimental study. Among the samples, there was a case where we purposely changed the machining conditions to achieve a high surface roughness value of $Ra \geq 3$ μm.

The shafts generally have higher surface roughness values than the hub specimens, whose values range from $1 \leq Ra \leq 3$ μm. Let's also inspect the shaft mounting diameter and other re-

maining dimensions using a digital micrometer and caliper with an accuracy of 0.001 mm and 0.01 mm, respectively.

There are two groups of interference values within the selected pairs of experimental specimens. Pairs No. 1, 2 have the same actual mean interference value, and the value of the three remaining one ranges from 42 μm to 45 μm. The selection of the mean value for the sample series starting at 33 μm involves the studies of the relative interference value. Let's initially consider this value at the particular rate of $\delta_m/d = 1.6$ ‰, which means increasing the occurrence probability of loss value L_p. Here, with $d = 20$ mm, $\delta_m = 32$ μm. **Table 2** displays the measured dimensional parameters of the specimens before and after coupling processes.

Fig. 2. Coordinate-measuring machine (CMM) and surface profiler

Table 2

Geometrical parameters before and after two assembly processes

Before assembly					
Pair No.	δ_m	d_o	l	Ra_s	Ra_h
	(μm)	**(mm)**	**(mm)**	**(μm)**	**(μm)**
1	33	29.91	14.54	1.24±0.02	0.53±0.01
2	33	29.92	14.53	2.98±0.09	3.35±0.06
3	42	29.92	14.41	2.68±0.08	0.83±0.01
4	45	29.89	14.50	2.35±0.04	0.67±0.01
5	47	29.94	14.41	1.01±0.03	0.76±0.01
After one coupling and decoupling process					
Pair No.	δ_m	d_o	l	Ra_s	Ra_h
	(μm)	**(mm)**	**(mm)**	**(μm)**	**(μm)**
1	33	29.91	14.54	1.07±0.02	0.14±0.01
2	33	29.92	14.53	3.02±0.15	0.83±0.12
3	42	29.92	14.41	2.92±0.06	0.15±0.01
4	45	29.89	14.50	2.43±0.04	0.11±0.01
5	47	29.94	14.41	0.95±0.05	0.12±0.01
After two coupling and decoupling processes					
Pair No.	δ_m	d_o	l	Ra_s	Ra_h
	(μm)	**(mm)**	**(mm)**	**(μm)**	**(μm)**
1	33	29.91	14.54	1.34±0.78	0.17±0.10
2	33	29.92	14.53	2.86±0.67	0.19±0.13
3	42	29.92	14.41	2.95±0.14	0.17±0.01
4	45	29.89	14.50	2.50±1.03	0.12±0.05
5	47	29.94	14.41	1.13±0.47	0.15±0.08

2. 3. Axial extraction test

Let's employ UTM to examine the maximum axial load that can be loaded, along with a respectively transitional displacement over time. Let's clean the parts with acetone before assembly, ensuring oil-free and impurity-free surfaces.

When mating, let's partially fix the shaft and hub with several jigs, which prevents the assembly parts from being deflected or unintentionally displaced. In addition to the fixture, it was necessary to use an extension part called a pestle, and the reason is our intention to assemble and disassemble the joint in the same loading stage. The dimensions and model are displayed in **Fig. 3**, **4**.

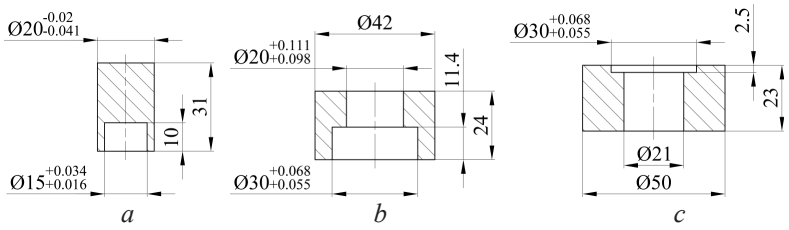

Fig. 3. Dimensions of fixtures used in extraction test:
a – pestle; *b* – upper jig; *c* – lower jig

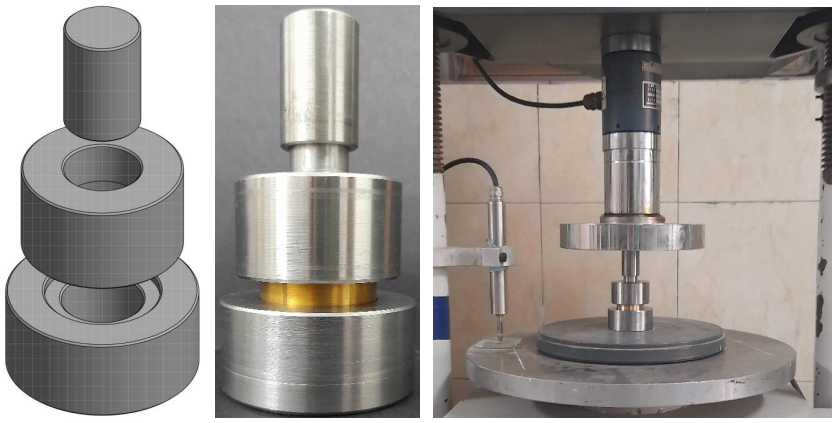

Fig. 4. 3D model and the actual mounting example of fixtures used in extraction test

3. Results and discussions

For pairs No. 1, 2, the actual mean interference value is maintained at $\delta_m = 33$ μm to highlight the effect of surface roughness on the overall load capacity. Specifically, the total value of shaft-hub surface roughness in pair No. 1 is smaller than that of pair No. 2, which corresponds to higher experimental axial load results.

Fig. 5, *b* shows a unique axial load test result, where the critical load of the third pair is more significant than those of the fourth and fifth joints. All of this confirms the phenomenon of interference loss due to plastic deformation of the joint. But for this steel-brass fit, the relative interference value is at $\delta_m/d = 2.25$ ‰.

Analyzing the results of the axial load test on the relative interference value $\delta_m/d = 2.25$ ‰, it is possible to divide the five pairs of samples into two groups, with and without loss of interference due to the deformation of the joint L_p. Based on (9) and the measurement results, also the obtained experimental parameters, it is possible to derive the following set of equations:

– without L_p:

$$\begin{cases} \text{Pair No.1: } 33 - a \cdot (1.24 + 0.53) = 29.21; \\ \text{Pair No.2: } 33 - a \cdot (2.98 + 3.35) = 26.03; \\ \text{Pair No.3: } 42 - a \cdot (2.68 + 0.83) = 35.88, \end{cases}$$

– with L_p:

$$\begin{cases}\text{Pair No.4: } 45 - a \cdot (2.35 + 0.67) - L_p = 30.06; \\ \text{Pair No.5: } 47 - a \cdot (1.01 + 0.76) - L_p = 31.87,\end{cases}$$

processing the equations, let's obtain the following set of results:

– without L_p:

$$\begin{cases} a = 2.141; \\ a = 1.101; \\ a = 1.744, \end{cases}$$

– with L_p:

$$\begin{cases} L_p = 11.618 \text{ µm}; \\ L_p = 11.413 \text{ µm}. \end{cases}$$

By analyzing the experimental results, there is an interference loss prediction formula for the case of steel-brass interference fit. First of all, the constant value a can be limited to $a = [1.1…2.1]$. Secondly, with loss value L_p, it is possible to see that the loss amount is about 20 % of the total interference value, or $L_p = 0.2 \cdot \delta_m$.

Finally, it is possible to attain the formula to predict the actual interference of the joint in two cases:

– without L_p:

$$\delta = \delta_m - [1.1…2.1] \cdot (Ra_s + Ra_h), \tag{10}$$

– with L_p:

$$\delta = \delta_m - [1.1…2.1] \cdot (Ra_s + Ra_h) - 0.2 \cdot \delta_m. \tag{11}$$

Fig. 6, *a* shows some fascinating results of the shaft surfaces. Due to the characteristics of the steel-brass material pair, the surface roughness values of the shaft samples are almost unaffected, in contrast to the hubs, which have a significant quantity of changes. Specifically, there are deformations of the asperities and mechanical adhesion between the contact surfaces due to the difference in the critical stress values of the material pair. It is also possible to also say that the better mating surface tears down the inferior one with fewer mechanical properties.

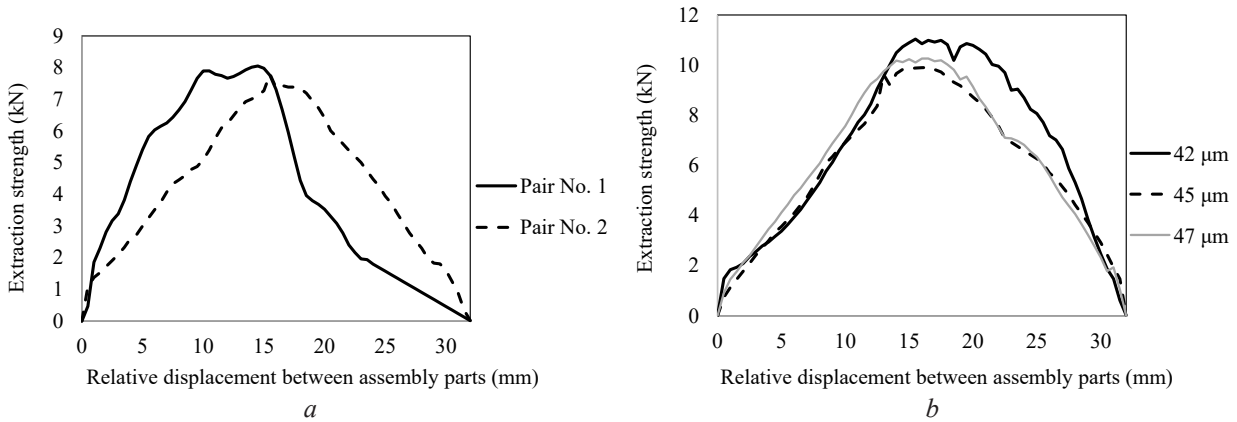

Fig. 5. Diagram of the extraction strength and the respective displacement between assembly parts: *a* – at $\delta_m = 33$ µm; *b* – at $\delta_m = 42$, 45, and 47 µm

The surface of the shaft detailed in **Fig. 7** appears to have many worn parts from the hub surface, one of the factors that change the hub surface roughness. Besides, this shows that con-

sidering the interference loss factor in this case of material pair is extremely important, directly affecting the efficiency of the fit properties.

It is possible to see that the higher the initial roughness value, the larger the number of changes, and these roughness values seem to reach a point where they cannot continue to change even under extreme pressure. In **Fig. 6, *b***, between the first and second assembly processes, the roughness value of pairs No. 1, 3, 4, and 5 is almost unchanged, which identifies that the hardening of the surface asperities occurs. The steel-brass material pair still follows several studies on the surface asperities hardening phenomenon [16, 20].

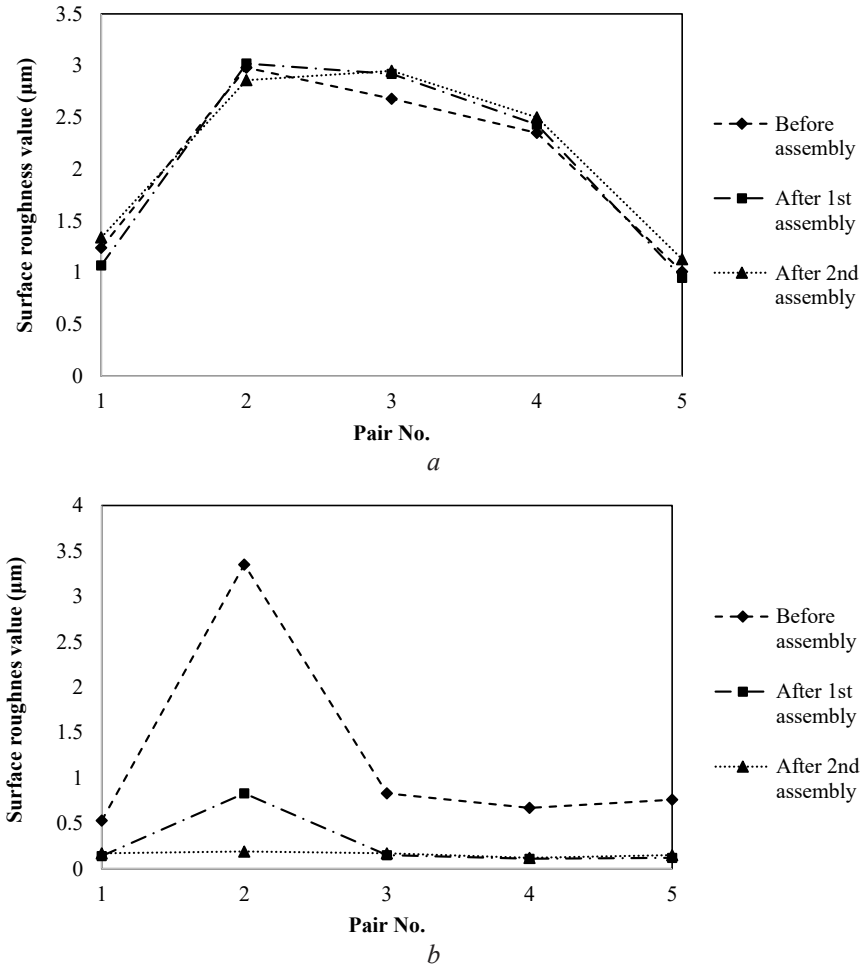

Fig. 6. Surface roughness value before and after two assembly processes:
a – shaft specimens; *b* – hub specimens

Fig. 7. Pair of assembled parts and shaft surface after disassembling

From the experiment, it is possible to confirm that the losses of the interference value originate from the plastic deformation, the surface hardening phenomenon, and the physical adhesions.

Although the motives are somewhat identical, the relative interference values are unalike between this and other practical cases. In steel-duralumin joints, the consideration is around 1.6 ‰ [17], and the experimental results of this steel-brass case show that it is 2.25 ‰.

Let's prove the difference between the standard interference fit and this particular steel-brass fit case by evaluating the actual loss factor a and the interference losses L_r, L_p. Accordingly, the load capability of steel-brass interference assembly is broadened. For instance, with nominal diameter $d = 20$ mm, when to limit the relative interference to the new value of 2.25 ‰, it is possible to select the theoretical interference value as high as 45 μm, whose conventional standards can only reach 30 μm.

For a more persuasive conclusion, it is necessary to recreate the experimental results with different assembly parameters while unchanging the material properties. After that, it is possible to replicate the experiment for other coupling materials to determine all the possibilities of the loss factor a and the interference loss values L_r, L_p.

4. Conclusions

The study has performed an analysis of interference fit considering the case of the steel-brass material pair. The specific characteristics of the mating surfaces have shown that mechanical adhesion occurs, tearing out the brass hub assembled surface. Consequently, this phenomenon directly affects the overall load capacity of the interference fit.

In addition, the relative interference value δ_m/d according to experimental results is different from the basic calculation standards [2, 3]. The loss due to deformation of the mating parts only appeared at 2.25 ‰. These results have broadened the range of load capacity response of steel-brass material pair in the design of interference joints. Moreover, for the comprehensive application of this result, more experimental procedures with more objective input parameters are required.

From the axial load test graphs, the relative sliding between the joints when nearly reaching the limit of load capacity occurs with a higher frequency than in the case of steel-steel interference fits. Therefore, in some cases, complex load-bearing or working environment with considerable impact factors will possibly affect the steel-brass interference fits.

The study also presents a new way of predicting the actual mean interference for steel-brass interference fit by determining the losses that depend on the surface roughness value, the influence of the deformation of coupling parts, and the phenomenon of surface hardening. The predictive loss coefficient a ranges from 1.1 to 2.1, different from the commonly chosen calculation standard, which is $a = 3$ [2, 3].

From these studies, the coefficients are given to support the calculation process of the interference fit of the steel-brass pair. The results help designers to choose the right interference fit with the goal of increasing service life and reducing costs. This interference fit is widely used in the field of mechanical engineering.

Conflict of interest

The authors declare that there is no conflict of interest in relation to this paper, as well as the published research results, including the financial aspects of conducting the research, obtaining and using its results, as well as any non-financial personal relationships.

Acknowledgement

This research is funded by VNU-HCM under grant number C2021-20-03. We acknowledge Ho Chi Minh City University of Technology (Vietnam, HCMUT), VNU-HCM for supporting this study.

References

[1] Timoshenko, S., Goodier, J. N. (1951). Theory of elasticity. McGraw Hill Book Company.

[2] German Institute for Standardisation (2017). Interference fits – Part 1: Calculation and design rules for cylindrical self-locking pressfits (DIN Standard No. 7190-1:2017-02). doi: http://doi.org/10.31030/2414563

[3] International Organization for Standardisation. (2010). Geometrical product specifications (GPS) – ISO code system for tolerances on linear sizes – Part 1: Basis of tolerances, deviations and fits (ISO Standard No. 286-1:2010). Available at: https://www.iso.org/standard/45975.html

[4] Wang, X., Lou, Z., Wang, X., Xu, C. (2017). A new analytical method for press-fit curve prediction of interference fitting parts. Journal of Materials Processing Technology, 250, 16–24. doi: http://doi.org/10.1016/j.jmatprotec.2017.06.022

[5] McMillan, M. D., Booker, J. D., Smith, D. J., Fedorciuc Onisa, C., Korsunsky, A. M., Song, X. et. al. (2016). Analysis of increasing torque with recurrent slip in interference-fits. Engineering Failure Analysis, 62, 58–74. doi: http://doi.org/10.1016/j.engfailanal.2015.12.005

[6] Zhao, J., Wang, J. X., Yu, C., Tang, S. Q., Yao, J. (2019). Influence of radial interference on torque capacity of shrink-fit camshaft. Advances in Mechanical Engineering, 11 (4), 168781401881764. doi: http://doi.org/10.1177/1687814018817640

[7] Simpson, N., Wrobel, R., Mellor, P. H., Booker, J. D. (2016). Multi-physics experimental investigation into stator-housing contact interface. 8th IET International Conference on Power Electronics, Machines and Drives (PEMD 2016). doi: http://doi.org/10.1049/cp.2016.0129

[8] Booker, J. D., Truman, C. E. (2011). Measuring the coefficient of friction for use in shrink-fit calculations. Experimental Techniques, 35 (2), 7–13. doi: http://doi.org/10.1111/j.1747-1567.2009.00593.x

[9] Pedersen, N. L. (2016). On optimization of interference fit Assembly. Structural and Multidisciplinary Optimization, 54 (2), 349–359. doi: http://doi.org/10.1007/s00158-016-1419-0

[10] Buczkowski, R., Kleiber, M. (2016). A study of the Surface Roughness in elasto-plastic shrink fitted joint. Tribology International, 98, 125–132. doi: http://doi.org/10.1016/j.triboint.2016.02.021

[11] Raj, A. P., Bhatti, A., Dhanish, P. B. (2020). Combined effect of cylindricity, roundness and roughness on axial load-carrying ability of interference fits. Proceedings of the Institution of Mechanical Engineers, Part J: Journal of Engineering Tribology, 234 (11), 1697–1711. doi: http://doi.org/10.1177/1350650120919883

[12] McMillan, M., Hendry, J. L., Woolley, A., Pavier, M. J. (2017). Measurement of partial slip at the interface of a shrink fit assembly under axial load. Experimental Mechanics, 58 (3), 407–415. doi: http://doi.org/10.1007/s11340-017-0359-y

[13] Biron, G., Vadean, A., Tudose, L. (2012). Optimal design of interference fit assemblies subjected to fatigue loads. Structural and Multidisciplinary Optimization, 47 (3), 441–451. doi: http://doi.org/10.1007/s00158-012-0836-y

[14] McMillan, M., Booker, J. D., Smith, D. J. (2011). Validation of micro-slip in interference fitted shafts subject to complex loading regimes. Applied Mechanics and Materials, 70, 351–356. doi: http://doi.org/10.4028/www.scientific.net/amm.70.351

[15] Hamrock, B. J., Schmid, S. R., Jacobson, B. O. (2013). Fundamentals of machine elements. CRC Press, 626. doi: http://doi.org/10.1201/b14229

[16] Tiwari, A., Almqvist, A., Persson, B. N. (2020). Plastic deformation of rough metallic surfaces. Tribology Letters, 68 (4). doi: http://doi.org/10.1007/s11249-020-01368-9

[17] Yang, G. M., Coquille, J. C., Fontaine, J. F., Lambertin, M. (2002). Contact pressure between two rough surfaces of a cylindrical fit. Journal of Materials Processing Technology, 123 (3), 490–497. doi: http://doi.org/10.1016/s0924-0136(02)00139-5

[18] German Institute for Standardisation. (2018). Bright steel products – Technical delivery conditions (German version EN Standard No. 10277:2018). doi: http://doi.org/10.31030/2803888

[19] German Institute for Standardisation. (2016). Copper and copper alloys – Rod for general purposes (German version EN Standard No. 12163:2016). doi: http://doi.org/10.31030/2535046

[20] Sun, F., Van der Giessen, E., Nicola, L. (2015). Effect of plastic flattening on the shearing response of metal asperities: A dislocation dynamics analysis. Journal of Applied Mechanics, 82 (7). doi: http://doi.org/10.1115/1.4030321

Received date 22.04.2022
Accepted date 25.07.2022
Published date 30.09.2022

How to cite: *Loc, N. H., Phong, L. V. (2022). Study of interference fit between steel and brass parts. EUREKA: Physics and Engineering, 5, 140–149. doi: http://doi.org/10.21303/2461-4262.2022.002524*